A methodology for snow data assimilation in a land surface model

Chaojiao Sun[1]

Hydrological Sciences Branch, Laboratory for Hydrospheric Processes, NASA Goddard Space Flight Center, Greenbelt, Maryland, USA

Goddard Earth Sciences and Technology Center, University of Maryland Baltimore County, Baltimore, Maryland, USA

Jeffrey P. Walker

Department of Civil and Environmental Engineering, University of Melbourne, Parkville, Victoria, Australia

Paul R. Houser

Hydrological Sciences Branch, Laboratory for Hydrospheric Processes, NASA Goddard Space Flight Center, Greenbelt, Maryland, USA

Received 11 May 2003; revised 4 March 2004; accepted 22 March 2004; published 27 April 2004.

[1] Snow cover has a large influence on heat fluxes between the land and atmosphere because of its high albedo and insulating thermal properties. Hence accurate snow representation in coupled land-ocean-atmosphere global climate models has the potential to greatly increase prediction accuracy. To this end, a one-dimensional extended Kalman filter analysis scheme has been developed to assimilate observed snow water equivalent into the NASA Seasonal-to-Interannual Prediction Project (NSIPP) catchment-based land surface model. This study presents the results from a set of data assimilation "twin" experiments using an uncoupled version of the land surface model. First, "true" snow states are generated by spinning-up the land surface model for 1987 using an observation-constrained version of the European Centre for Medium-Range Weather Forecasts (ECMWF) 15-year Re-Analysis (ERA-15) data set for atmospheric forcing. A degraded 1987 simulation was then made by initializing the model with no snow on 1 January 1987. A third simulation assimilated the synthetically generated snow water equivalent "observations" from the true simulation into the degraded simulation once a day. This study illustrates that by assimilating snow water equivalent observations, which are readily available from remote sensing satellites, other state variables (i.e., snow depth and temperature) can be retrieved and effects of poor initial conditions removed. Runoff and atmospheric flux predictions are also improved. *INDEX TERMS:* 1863 Hydrology: Snow and ice (1827); 3260 Mathematical Geophysics: Inverse theory; 3322 Meteorology and Atmospheric Dynamics: Land/atmosphere interactions; 3337 Meteorology and Atmospheric Dynamics: Numerical modeling and data assimilation; 3360 Meteorology and Atmospheric Dynamics: Remote sensing; *KEYWORDS:* snow assimilation, extended Kalman filter, GCM initialization

Citation: Sun, C., J. P. Walker, and P. R. Houser (2004), A methodology for snow data assimilation in a land surface model, *J. Geophys. Res.*, *109*, D08108, doi:10.1029/2003JD003765.

1. Introduction

1.1. Importance of Snow

[2] Snow plays an important role in governing the Earth's global energy and water budgets, as a result of its high albedo, low thermal conductivity, and considerable spatial and temporal variability [*Hall*, 1998]. Snow cover is one of the most highly varying hydrological quantities on the Earth's surface [*Gutzler and Rosen*, 1995], with the Northern Hemisphere mean monthly snow covered land area ranging from about 7% to 40% during the annual cycle [*Hall*, 1988]. Moreover, the energy demanded by snowmelt can significantly cool the surface and the overlying air [*Dewey*, 1977; *Namias*, 1985; *Baker et al.*, 1992; *Groisman et al.*, 1994]. Thus surface air temperature forecasts from numerical weather prediction are very sensitive to the snow cover extent and thickness. For example, improvement of snow physics in the NCEP (National Centers for Environmental Prediction) ETA operational forecast model substantially reduced a 2 m daytime air temperature cold bias for snow covered areas [*Mitchell et al.*, 2002]. Further, snow covered landscapes adjacent to bare soil regions have been found to produce mesoscale wind circulations [*Johnson et al.*, 1984] and snow cover variability has been shown to affect climate patterns in coupled climate simulations. Using

[1]Now at Global Modeling and Assimilation Office, NASA Goddard Space Flight Center, Greenbelt, Maryland, USA.

0148-0227/04/2003JD003765$09.00

the NESDIS (National Environmental Satellite, Data, and Information Service) snow cover data [*Robinson et al.*, 1993], *Cohen and Entekhabi* [1999] demonstrate that early season Eurasian snow cover variations are associated with dominant modes of midlatitude variability in the Northern Hemisphere winter. In addition, recent observational studies [*Lo and Clark*, 2002; *Bamzai and Shukla*, 1999] have shown an inverse relationship between antecedent snow mass or snow cover extent and Asian and North American summer monsoon intensity. Hence any long term coupled climate system prediction is dependent on accurate snow information.

[3] Because of its low thermal conductivity, snow can insulate the underlying soil and impede the depth and severity of soil freezing [*Lynch-Stieglitz*, 1994; *Sud and Mocko*, 1999]. While the energy balance is the primary driver of the Earth's atmospheric circulation system and associated climate, the water budget is also significantly modified through snowmelt processes. Being a medium-term water store, snow plays an important role in springtime runoff generation and flood production [*Hall*, 1988], and can provide a substantial component of the annual water budget. In many northern latitude regions (e.g., California), spring meltwater from the winter snowpack is the greatest source of water in the annual soil moisture budget [*Aguado*, 1985]. Therefore, to achieve accurate runoff and soil moisture prediction, which provides feedback to climate prediction [*Koster and Suarez*, 1995], it is important to accurately initialize snow cover in climate model forecasts.

1.2. Snow Observations

[4] Owing to considerable subgrid-scale spatial and temporal snow variability, and deficiencies in model snow physics, realistic global climate model snow prediction is difficult [*Liston et al.*, 1999]. Any land surface model initialization based solely on model spin-up will be affected by these problems. While there is a demonstrated need for routine snow observation (snow water equivalent, snow depth, snow temperature and hence snow cover), particularly for climate model initialization, routine ground-based snow observations are uncommon. In the United States, daily snow depth measurements are available at airports and from a network of volunteer observers. Snow course and SNOTEL (Snowpack Telemetry) sites collect more detailed snow data (snow depth, snow water equivalent and snow temperature), but these data are only collected in remote areas of the mountainous western states (information on SNOTEL can be found on the following Web site: http://www.wcc.nrcs.usda.gov/snotel/). In Canada, daily ground-based snow depth observations have been made at most synoptic stations since the 1950s, but the observing network is concentrated over the southern, more populated regions. Snow course observations are widely distributed throughout all of the provinces and territories, but they are made infrequently (weekly, biweekly or monthly) [*Brown et al.*, 2003]. Even though the in situ North American observations are among the best in the world, they are insufficient for global climate model initialization due to extreme snow depth heterogeneity.

[5] In contrast, remote sensing has the capability for providing snow information with the spatial coverage and temporal resolution needed for global climate model initialization. Remote sensing observations average out the small-scale variability inherent to in situ snow observations, therefore producing better climate-relevant snow information. Operational weekly snow cover analyses over North America have been produced from visible satellite observations by NOAA since 1966 [*Robinson et al.*, 1993]. Although this is the longest remotely sensed snow record available, it only provides the snow cover rather than snow mass information. While visible-infrared satellite sensors, such as the Moderate Resolution Imaging Spectroradiometer (MODIS) onboard Terra and Aqua currently provide the highest daily snow cover spatial resolution (500 m), they only work for cloud-free conditions. These high-resolution observations can provide information on fractional coverage of snow, which complements passive microwave observations that have coarser resolution, but fractional snow cover observation alone is difficult to use for quantitative snowpack initialization. Infrared sensors can also provide surface skin temperature information for cloud free areas. However, these temperature observations may not represent the surface snow temperature, especially when vegetation protrudes above the snowpack. When high-resolution snow cover and surface skin temperature observations are used together with snow mass observations from passive microwave sensors, synergistic benefits may be derived for estimating snowpack states. Since research-quality data sets of simultaneous snow cover, snow depth, and snow water equivalent observations are still under development [*Robinson*, 2002], we focus on using passive microwave observations in this study.

[6] Passive microwave sensors can measure snow mass (snow water equivalent) under both nighttime and cloudy (nonprecipitating) conditions, which persist during much of the high latitude snow season. Since November 1978, the Scanning Multichannel Microwave Radiometer (SMMR) and the Special Sensor Microwave Imager (SSM/I) have been acquiring passive microwave observations. SMMR observations (resampled to $^1/_4$ degree by $^1/_4$ degree resolution) are available from 1978 to 1987, and SSM/I observations (resampled to $^1/_2$ degree by $^1/_2$ degree resolution) are available since 1987. With the launch of the Earth Observing System (EOS) Aqua satellite in May 2002, high-quality passive microwave snow water equivalent observations are available from its Advanced Microwave Scanning Radiometer for EOS (AMSR-E) instrument. AMSR-E is a passive microwave radiometer expected to produce 10 km resolution snow water equivalent observations.

[7] *Chang et al.* [1987] have developed a commonly used algorithm to derive snow water equivalent and snow depth from passive microwave data based on a radiative transfer model with several assumptions. They assumed that snow crystal size remains constant (0.3 mm) throughout the season. In reality, snow crystals evolve with the season and weather conditions [*Foster et al.*, 1997], and their size is the most important factor in determining the algorithm accuracy. Vegetation cover can also impose large uncertainties in passive microwave snow water equivalent estimation. For instance, *Brown et al.* [2001] showed that the boreal forest snowpack mass estimated from passive microwave observations was consistently underestimated. In a recent study, J. L. Foster et al.

(Quantifying the uncertainty in passive microwave snow water equivalent observations, submitted to *Remote Sensing of Environment*, 2004) have addressed these uncertainties and estimated errors in snow water equivalent observations derived from passive microwave measurements, based on snowpack age, climate, vegetation, topography, and brightness temperature measurement error. When the snowpack is wet, snow information is difficult to extract from passive microwave radiometry. Therefore only nighttime satellite overpasses are commonly examined, as there is a higher probability that the snowpack is not actively melting at night. Information on snowpack melt status, though not used in this study, could be used to further constrain model snow dynamics.

1.3. Snow Assimilation

[8] The few studies that have constrained model predictions with snow observations have generally replaced the modeled snow states with observations directly; this assimilation method is commonly called ''direct insertion.'' For example, *Liston et al.* [1999] used this approach successfully in identifying deficiencies in a regional climate model associated with snow distribution, and *Rodell et al.* [2004] have used direct insertion to assimilate MODIS snow cover observations into the Global Land Data Assimilation System (GLDAS). J. Jin and N. L. Miller (An analysis of climate variability and snowmelt mechanisms in mountainous regions, submitted to *Journal of Hydrometeorology*, 2003) also used this technique to investigate snowpack impact on climate variability and snowmelt mechanisms in mountainous regions.

[9] Direct insertion assumes that observations are perfect, and model forecasts do not contain useful information. However, the reality is that model prediction can sometimes be more accurate than observations; for example, model-predicted snow depth can be more accurate than remotely sensed observations in densely vegetated areas. The propagation of information to coupled state variables in direct insertion is accomplished only through model physics. B. A. Cosgrove and P. R. Houser (Impact of surface forcing biases on snow assimilation, submitted to *Journal of Hydrometeorology*, 2003) found that large water balance errors occur when imperfectly modeled snow melting processes interact with the direct insertion of perfect snow observations. Constraining these biases in assimilation systems is important for achieving optimal assimilation results [*Dee and da Silva*, 1998; *Dee and Todling*, 2000], and is an important topic for future research.

[10] An improvement on direct insertion is the statistical interpolation scheme (also called optimal interpolation). *Brasnett* [1999] used this scheme to assimilate snow depth observations from synoptic stations into a very simple snow accumulation, aging and melt model driven by numerical weather prediction precipitation forecasts and screen-level temperature analyses. The resulting global snow depth analysis was found to be more accurate than a climatological estimate. Recently, *Brown et al.* [2003] applied this method to generate a gridded monthly snow depth and snow water equivalent data set for North America, using snow depth observations from the United States cooperative stations and Canadian climate stations. They found that the gridded results agreed well with in situ and satellite data over midlatitudinal regions during the AMIP II (Atmospheric Model Intercomparison Project II) period (1979–1996). These results provide impetus for the development of advanced assimilation methods and satellite observations to produce accurate snow fields for global climate model initialization.

[11] In this study, we use the statistical Kalman filter approach to assimilate snow water equivalent observations, which accounts for relative observation and prediction uncertainty to produce a statistically optimal estimate. We study the assimilation of satellite snow water equivalent observations made by passive microwave sensors, because snow water equivalent is crucial for estimating water fluxes in hydrologic models and surface albedo in numerical weather prediction models [*Robinson and Kukla*, 1985]. Moreover, it is the total mass (i.e., snow water equivalent, which is the product of snow depth and density) in the snowpack that directly determines its passive microwave response; this is the basis for passive microwave snow water equivalent estimation. Thus for this study we only assimilate remotely sensed snow water equivalent, and allow the model to predict the snow density evolution. While directly replacing snow model state variables with observations is possible, this does not account for the relative prediction and observation errors, and does not provide a framework for correcting the nonobserved but highly correlated snow depth and heat content model state variables.

[12] This study explores how routinely available passive microwave snow water equivalent observations can be assimilated efficiently into a state-of-the-art land surface model with a physically based snow submodel, using the extended Kalman filter. This methodology is developed through a series of numerical experiments using synthetic model-generated snow water equivalent observations. It is shown that sequential snow water equivalent assimilation can also retrieve the snow depth and snow temperature fields, and that runoff and atmospheric flux predictions are improved.

2. Models

2.1. Land Surface Model

[13] This study uses the NASA Seasonal-to-Interannual Prediction Project (NSIPP) catchment-based land surface model of *Koster et al.* [2000], which abandons the traditional rectangular land surface discretization approach in favor of topographically based hydrological catchment elements. The model includes an explicit subcatchment-scale soil moisture and evaporation variability treatment where each catchment is divided into three regimes: saturated, stressed (wilting) and unstressed. In this application about 5000 catchments are used to model the North American continent, with an average catchment size of 3600 km^2.

[14] The forcing data for the catchment-based land surface model, including air temperature and humidity at 2 m height, wind speed at 10 m height, total and convective precipitation, downward solar and longwave radiation, and atmospheric pressure, were derived from the 15-year (1979–1993) ECMWF Re-Analysis (ERA-15) that was scaled to match monthly averaged meteorological

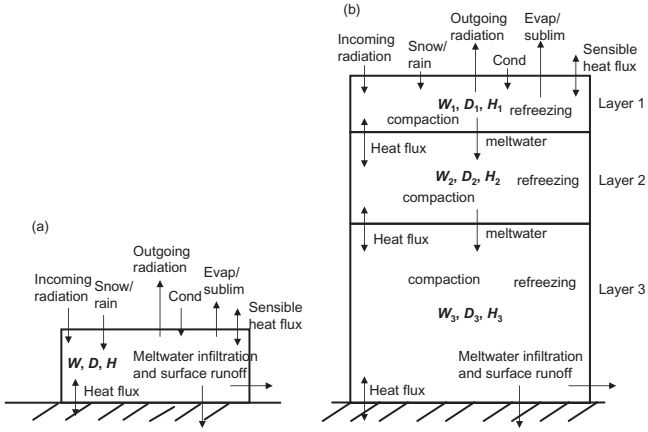

Figure 1. Snow model schematic: (a) Single-layer mode (when snow coverage <1). (b) Three-layer mode (when snow coverage = 1 and total snow water equivalent $W_T >$ 13 mm).

observations [*Berg et al.*, 2003]. Initial conditions were obtained from "spinning-up" the catchment-based land surface model by iterating the model over the same year of atmospheric forcing for 10 years, by which time most catchments had reached equilibrium. The topographic, soil and vegetation parameter specifications are the same as in the work of *Walker and Houser* [2001], with the catchment boundaries and topographic parameters derived from a 30 arc second (about 1 km) digital elevation model of North America [*Ducharne et al.*, 2000]. The soil and vegetation parameters are from the first International Satellite Land Surface Climatology Project (ISLSCP) initiative [*Sellers et al.*, 1996].

2.2. Snow Submodel

[15] The catchment-based land surface model includes the *Lynch-Stieglitz* [1994] snow submodel. This physically based snow model accounts for snowpack evaporation, sublimation, condensation, radiation interactions, precipitation as rain or snowfall depending on the air temperature, snowmelt, and metamorphosis [see also *Stieglitz et al.*, 2001]. The snow model operates in both single-layer and three-layer modes, depending on the snowpack depth, with three prognostic variables per layer (see Figure 1): snow water equivalent W, snow depth D (a function of snowpack density ρ and W) and heat content H (a function of W and snow temperature T).

[16] To eliminate numerical problems associated with extremely thin snowpacks and to ensure a smooth transition from snow-free to complete snow coverage, the snow model makes use of a single snow layer, a fractional snow coverage factor α, and a critical minimum total snow water equivalent value W_c of 13 mm (equivalent to a 87 mm fresh snowpack with a 150 kg/m^3 density). As snow accumulates, the single layer snowpack is assumed to grow horizontally from a no snow condition ($\alpha = 0$) with W_c to complete snow coverage ($\alpha = 1$). Once there is complete coverage (W_c = 13 mm and $\alpha = 1$), the snowpack grows vertically. Likewise, during snowmelt or sublimation, the snow model reverts to a single-layer mode once total snow water equivalent W_T reduces to 13 mm (typically equivalent to a 65 to 43 mm deep mature snowpack corresponding to a density of 200 kg/m^3 to 300 kg/m^3) for $\alpha = 1$, and then begins to decrease α toward 0 for this fixed W_T of 13 mm. In the single-layer mode, the snow model outputs homogeneous density and temperature information for all three layers (for consistency), with the layer depths as defined below.

[17] During periods when the catchment is completely covered with snow ($W_T \geq 13$ mm), the snow model operates in the three-layer mode, with separate physics for each layer. To capture the diurnal surface radiating temperature range, imposed snow depth geometry is applied at each time step. The layering geometry is set to keep the first layer (indexed from top to bottom such that layer 1 interacts with the atmosphere and layer 3 interacts with the soil) thin ($D_1 \leq$ 0.05 m), and remaining snow partitioned between the second and third layers to best represent the temperature gradients within the snowpack.

[18] The specific snow depth modeling rules are as follows. For the total catchment snowpack depth $D_T = D_1 + D_2 + D_3$, for the three-layer mode ($\alpha = 1$), the depth of each layer is:

$$\begin{cases} D_1 = 0.05\,\mathrm{m} \\ D_2 = 0.34(D_T - 0.05) \\ D_3 = 0.66(D_T - 0.05) \end{cases} \quad \text{if } D_T > 0.2\,\mathrm{m} \qquad (1)$$

$$\begin{cases} D_1 = 0.25\,D_T \\ D_2 = 0.50\,D_T \\ D_3 = 0.25\,D_T \end{cases} \quad \text{if } D_T \leq 0.2\,\mathrm{m}. \qquad (2)$$

[19] For single-layer mode (i.e., $\alpha < 1$), only (2) is used for the layer depths. Thus at the end of each time step the snow layer boundaries are moved, with the associated snow water equivalent and heat content variables redistributed accordingly. This process is required to: (1) maintain a thin surface layer that insulates the lower layers from atmospheric cooling; (2) maintain a thin lower snow layer for small snowpacks ($D_T \leq 0.2$ m), to deal with large snow-soil temperature gradients, and a thicker lower snow layer for large snowpacks ($D_T > 0.2$ m) when snow-soil temperature gradients are expected to be small; and (3) assure that model snow layers do not inadvertently disappear during melting and sublimation.

3. Assimilation Method

3.1. Extended Kalman Filter

[20] We use the extended Kalman filter (EKF) to assimilate total snow water equivalent observations into the NSIPP land surface model, because the Kalman filter explicitly takes into account the dynamical nature of model and observation errors, which evolve with time, to produce a statistically optimal model state estimates for linear systems [*Gelb*, 1974]. It also provides a framework to account for model and forcing biases. When the model is nonlinear, the EKF predicts model error covariance with

linearized model dynamics, and advances model states according to the full nonlinear model. The EKF has been widely used in atmospheric and ocean models [e.g., *Ghil and Malanotte-Rizzoli*, 1991; *Fukumori et al.*, 1999; *Verron et al.*, 1999; *Keppenne*, 2000], coupled ocean-atmosphere models [e.g., *Sun et al.*, 2002], and land surface models [e.g., *Walker and Houser*, 2001]. *Miller et al.* [1994] discuss a number of distinct Kalman filter extensions to nonlinear systems.

[21] To facilitate our discussions, we briefly describe the EKF equations here. The EKF consists of two steps. First, the model integrates forward in time to produce "forecast" states $\mathbf{x}^{\mathrm{f}}$ and their expected uncertainty $\mathbf{P}^{\mathrm{f}}$, based on the best estimate of the state variables $\mathbf{x}^{\mathrm{a}}$ and their uncertainty $\mathbf{P}^{\mathrm{a}}$ at the last time step. Second, when an observation is available, the model forecast and its uncertainty is "updated". The state variables are updated by adding to the forecast states the difference between the forecast and actual observation, weighted by the Kalman gain $\mathbf{K}$. Using the "unified notation" of *Ide et al.* [1997], the EKF forecasting equations are

$$\mathbf{x}^{\mathrm{f}}(t_k) = M_{k-1}[\mathbf{x}^{\mathrm{a}}(t_{k-1})] \tag{3}$$

$$\mathbf{P}^{\mathrm{f}}(t_k) = \mathbf{M}_{k-1}\mathbf{P}^{\mathrm{a}}(t_{k-1})\mathbf{M}_{k-1}^{\mathrm{T}} + \mathbf{Q}_{k-1}, \tag{4}$$

where M is the nonlinear model function, $\mathbf{M}$ is the linearized model operator, $\mathbf{P}$ is the forecast error covariance, and $\mathbf{Q}$ is the model error covariance. The superscripts "a" and "f" denote "analysis" and "forecast" steps, and the superscript "T" denotes the "transpose" operator.

[22] The best estimate of the system state vector $\mathbf{x}^{\mathrm{a}}$ and associated covariances $\mathbf{P}^{\mathrm{a}}$ are updated by

$$\mathbf{x}^{\mathrm{a}}(t_k) = \mathbf{x}^{\mathrm{f}}(t_k) + \mathbf{K}_{\mathrm{k}}\mathbf{d}_{\mathrm{k}} \tag{5}$$

$$\mathbf{P}^{\mathrm{a}}(t_k) = (\mathbf{I} - \mathbf{K}_{\mathrm{k}}\mathbf{H}_{\mathrm{k}})\,\mathbf{P}^{\mathrm{f}}(t_k), \tag{6}$$

where $\mathbf{K}$ is the Kalman gain matrix,

$$\mathbf{K}_{\mathrm{k}} = \mathbf{P}^{\mathrm{f}}(t_k)\mathbf{H}_{\mathrm{k}}^{\mathrm{T}}\left[\mathbf{H}_{\mathrm{k}}\mathbf{P}^{\mathrm{f}}(t_k)\mathbf{H}_{\mathrm{k}}^{\mathrm{T}} + \mathbf{R}_{\mathrm{k}}\right]^{-1}, \tag{7}$$

and $\mathbf{d}_{\mathrm{k}}$ is the so-called "innovation vector," which is the difference between the observed value and model-predicted value at an observing location,

$$\mathbf{d}_{\mathrm{k}} = \mathbf{y}_{\mathrm{k}} - H_{\mathrm{k}}\left[\mathbf{x}^{\mathrm{f}}(t_k)\right], \tag{8}$$

and $\mathbf{y}$ is the observation vector, $\mathbf{R}$ is the observation error covariance, H is the observation function, and $\mathbf{H}$ is the linearized approximation of the observation function H.

3.2. Application of the Extended Kalman Filter

[23] In this study, we use a one-dimensional extended Kalman filter to assimilate total snow water equivalent observations without considering spatial correlations between neighboring catchments. Since we use a one-dimensional land surface model, the only spatial correlation among state variables is through large-scale (greater than 50 km) atmospheric forcing correlation. Therefore a one-dimensional filter is a safe assumption for this study and yields substantial computational savings.

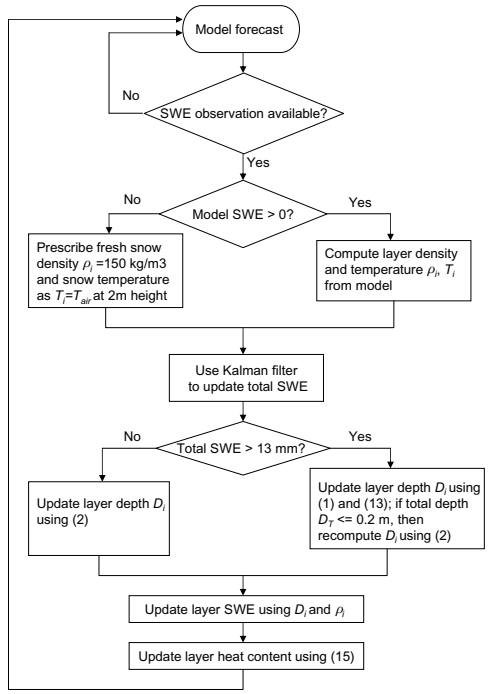

Figure 2. Flowchart showing assimilation procedure.

[24] In principle, it is possible to make corrections to the unobserved prognostic state variables (i.e., snow depth and heat content) by using the Kalman filter update equations (through the cross-correlation information contained in the forecast model covariances), since snow depth (a function of snowpack density and snow water equivalent) and heat content (a function of snow temperature and snow water equivalent) are strongly correlated with snow water equivalent. However, because of the somewhat arbitrary nature of the snow model layer geometry and its evolution (snow model layers appear and disappear, and snow mass is arbitrarily redistributed between layers as snowpack evolves), the correlations estimated from the model numerics were not well defined and this approach to update unobserved model states through the Kalman filter was abandoned.

[25] Instead, we use the Kalman filter to update model total snow water equivalent from observations, and rely upon the model physics to incorporate this highly correlated information into the snow depth and heat content variables. Since snowpack density and temperature (diagnostic variables) are not strongly correlated with total snow water equivalent, we assume they do not change immediately following a total snow water equivalent update, and use the model-predicted density and temperature to update the snow depth and heat content. When snow is observed but not predicted by the model, no snow density and temperature estimates are available from the model. In that case, we estimate the snow density to be 150 kg/m^3 (fresh snow) and use the 2-m air temperature as the snow temperature to update snow depth and heat content.

[26] Figure 2 shows a flowchart of the assimilation procedure. At each time step, a check is made to see if

the observation SWE is available. If not, the model integrates one time step forward. If an observation is available, snow density and temperature in each layer are computed. Density ρ_i in layer i is calculated as

$$\rho_i = \rho_w W_i/(D_i\alpha), \tag{9}$$

where $\rho_w = 1000$ kg/m^3 is the liquid water density and α is the catchment fractional snow cover. The temperature T_i and fraction of ice $f_{I,i}$ are also diagnosed as

$$\begin{cases} T_i = 0 \\ f_{I,i} = -H_i/(\rho_w L_f W_i) \end{cases} \quad \text{if } H_i + \rho_w L_f W_i \geq 0 \tag{10}$$

and

$$\begin{cases} T_i = (H_i + f_{I,i}\,\rho_w\,L_f\,W_i)/(C_{v,i}\,D_i\,\alpha) \\ f_{I,i} = 1.0 \end{cases} \quad \text{if } H_i + \rho_w\,L_f\,W_i < 0, \tag{11}$$

where L_f is the heat of fusion (J kg^{-1}), and $C_{v,i}$ is the heat capacity of snow in layer i (J Kg^{-1} K^{-1}). $C_{v,i}$ is derived from the heat capacity of ice as in the work of *Verseghy* [1991, equation (29)],

$$C_{v,i} = C_{v,ice}(\rho_i/\rho_{ice}), \tag{12}$$

where $C_{v,ice} = 2062$ J Kg^{-1} K^{-1}, and ρ_{ice} is the ice density, $\rho_{ice} = 920$ kg/m^3.

[27] The Kalman filter is then used to assimilate total snow water equivalent W_T ($W_T = W_1 + W_2 + W_3$). The fractional snow cover α is updated as soon as W_T has been updated ($\alpha = W_T/W_c$). If the three-layer mode is required ($\alpha = 1$), then snow depths and layer thicknesses are updated by the relationship

$$\alpha(\rho_1 D_1 + \rho_2 D_2 + \rho_3 D_3) = \rho_w W_T, \tag{13}$$

using the appropriate substitution for D_i from (1) or (2). The original snow density estimates and computed layer thicknesses are then used to compute the updated snow water equivalent for each layer by

$$\rho_w W_i = \alpha \rho_i D_i. \tag{14}$$

Likewise, the updated snow water equivalent and original temperature estimates are used to compute the heat content for each layer from

$$H_i = T_i C_{v,i} D_i \alpha - f_{I,i} L_f W_i. \tag{15}$$

[28] If the relationship between W_T and the threshold value for full snow coverage W_c deems that the snow model should be in single-layer mode ($W_T < W_c$), i.e., $\alpha < 1$, the single-layer snow depth and heat content are computed directly from the updated total snow water equivalent W_T using (14) and (15).

4. Numerical Experiments

[29] We undertook a set of numerical "twin" experiments to develop the method to assimilate daily snow water equivalent "observations" in North America. The "observation" and evaluation data used in this study were generated from model output. The "twin" experiment is an important first step in the development of a data assimilation system. These types of experiments allow us to determine the feasibility of the assimilation approach under known conditions, namely the "truth." This paper shows how through the assimilation of snow water equivalent observations, the snow depth and heat content can also be retrieved. By using a perfect model with perfect forcing and observations, we can clearly demonstrate how snowpack state variables may be retrieved when the initial conditions are poorly known. Testing of this methodology using remotely sensed snow water equivalent observations from both SMMR and SSM/I is the focus of a subsequent paper.

[30] The North American temporal and spatial snowpack evolution used here was generated by the catchment-based land surface model using the parameter specification, forcing data and spin-up initial conditions described above. This simulation provided the "truth" data for evaluation of our numerical experiments (hereafter referred to as the "truth" run) and the "observation" data for assimilation. To mimic the remotely sensed passive microwave snow observations, the daily total snow water equivalent from the truth run was taken as our observation. The data used to evaluate the assimilation included snow water equivalent, snow depth, snow density, snow temperature, snow cover fraction, upward short- and long-wave radiation, as well as runoff and evapotranspiration from the truth run.

[31] The truth run is contrasted with a degraded simulation to illustrate snowpack initialization error impact on snow state and atmospheric flux prediction, and the Kalman filter efficiency to correct poor snow state and atmospheric flux predictions. This simulation (hereafter referred to as the "open loop" run) used the same model, parameters and atmospheric forcing as the truth run, but with degraded initial conditions. The initial conditions are identical to the spin-up described above, with the exception that all snowpack memory was erased on 1 January 1987 (i.e., it was prescribed that no snow existed anywhere even though it was in the middle of the snow season). We could have used snow climatology as the initial condition, but we choose this extreme condition to illustrate the robustness of our assimilation scheme.

[32] The extended Kalman filter assimilation experiment (hereafter referred to as the "assimilation run") started with the same degraded initial conditions as the open loop run, assimilating one total snow water equivalent observation per day. Note that availability of daily observations is not a requirement of the EKF; observations can be assimilated in EKF whenever they become available. To undertake the Kalman filter assimilation, the linearized model function **M** and knowledge of model and observation error statistics are required (see equations 4, 5, 6 and 7). We compute **M** using a numerical approximation (forward finite difference) to the snow prognostic Jacobian matrix. Since we only use the Kalman filter to update total snow water equivalent, we only need to forecast the total snow water equivalent variance and not the covariances between all nine snow prognostic variables. Hence only the total snow water

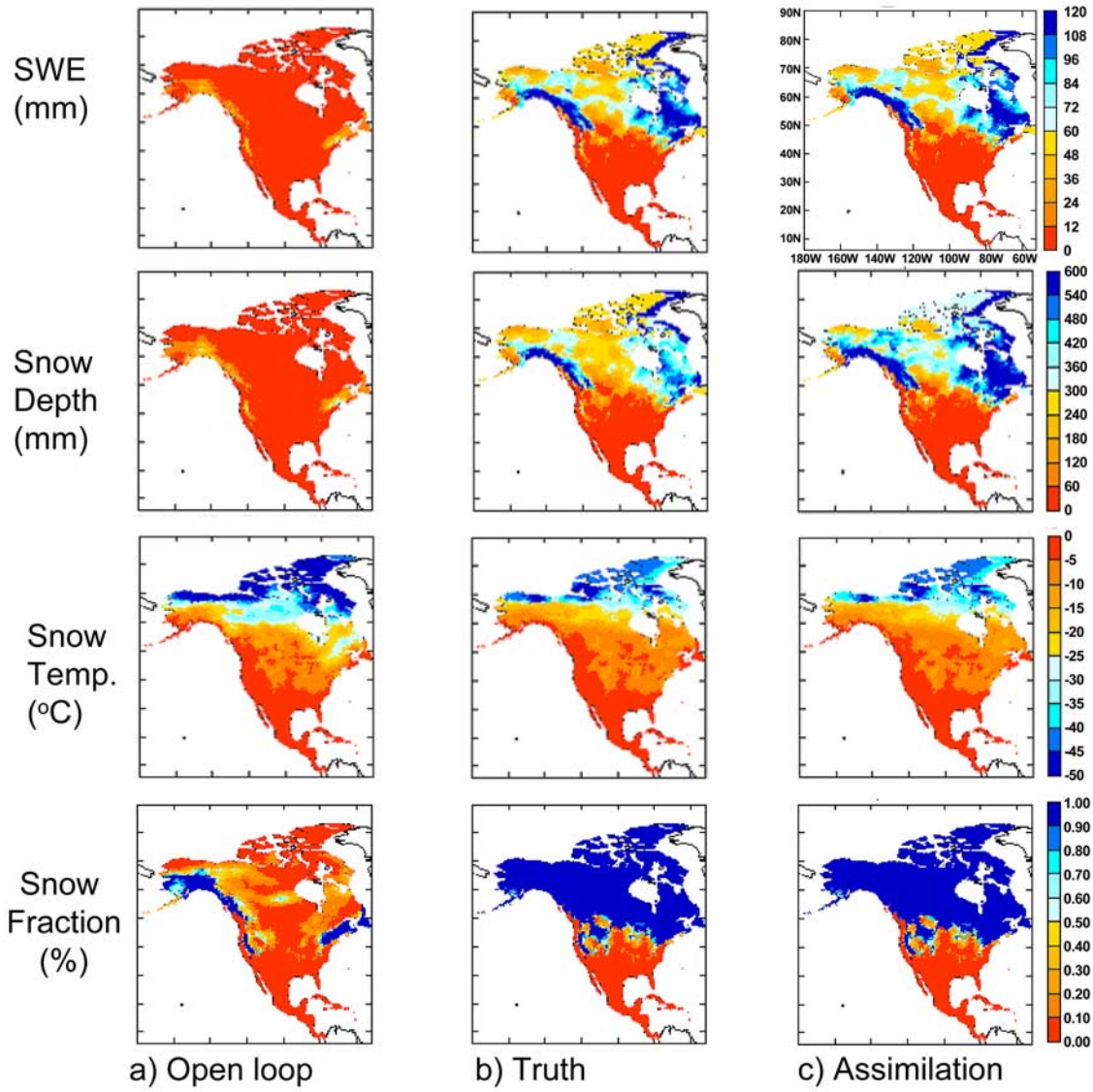

Figure 3. Snow simulation comparisons on 5 January 1987 over North America for snow water equivalent (in mm, top row); snow depth (in mm, second row); average temperature (in °C, third row); and areal snow fraction (bottom row) from (a) open loop run (with degraded initial condition), (b) truth run (using spin up initial condition), and (c) assimilation (with degraded initial condition and assimilation of daily total snow water equivalent observations).

equivalent Jacobian (now reduced to a scalar) needs to be calculated.

[33] The error statistics, including model error covariances **Q**, initial forecast error $\mathbf{P}^f$ (at time $t = 0$), and observation error covariances **R**, are specified as following. We used an initial $(20\ \text{mm})^2$ variance of model forecast error variance $\mathbf{P}^f$, a $(10\ \text{mm})^2$ model error variance **Q**, and a $(5\ \text{mm})^2$ total snow water equivalent observation error variance **R**. Note that these variances are only used in the EKF, while the "truth" and "observations" in the twin experiments do not include additional added noises.

5. Results and Discussion

[34] Figures 3 and 4 compare snowpack forecasts from the open loop, assimilation and truth runs near the start of January and middle of February, respectively. Figures 3a and 4a shows the impact of degraded snowpack initial condition on snow forecast in the open loop run, as compared to the truth run in Figures 3b and 4b. In contrast, the assimilation scheme recovered the snow water equivalent, snow temperature and snow fraction after only five days of assimilation; see Figures 3c and 4c. Note the snow depth in the assimilation run is overestimated initially (Figure 3). That is because we depend on the model to provide a snow density estimate. With the degraded initial condition, the assimilation run starts with the default 150 kg/m^3 fresh snow density, which is lower than the mature snowpack density. After one-and-half months, snow depth from the assimilation run has been recovered (Figure 4), since the density value becomes closer to the true value as the assimilation progresses. In contrast, snow

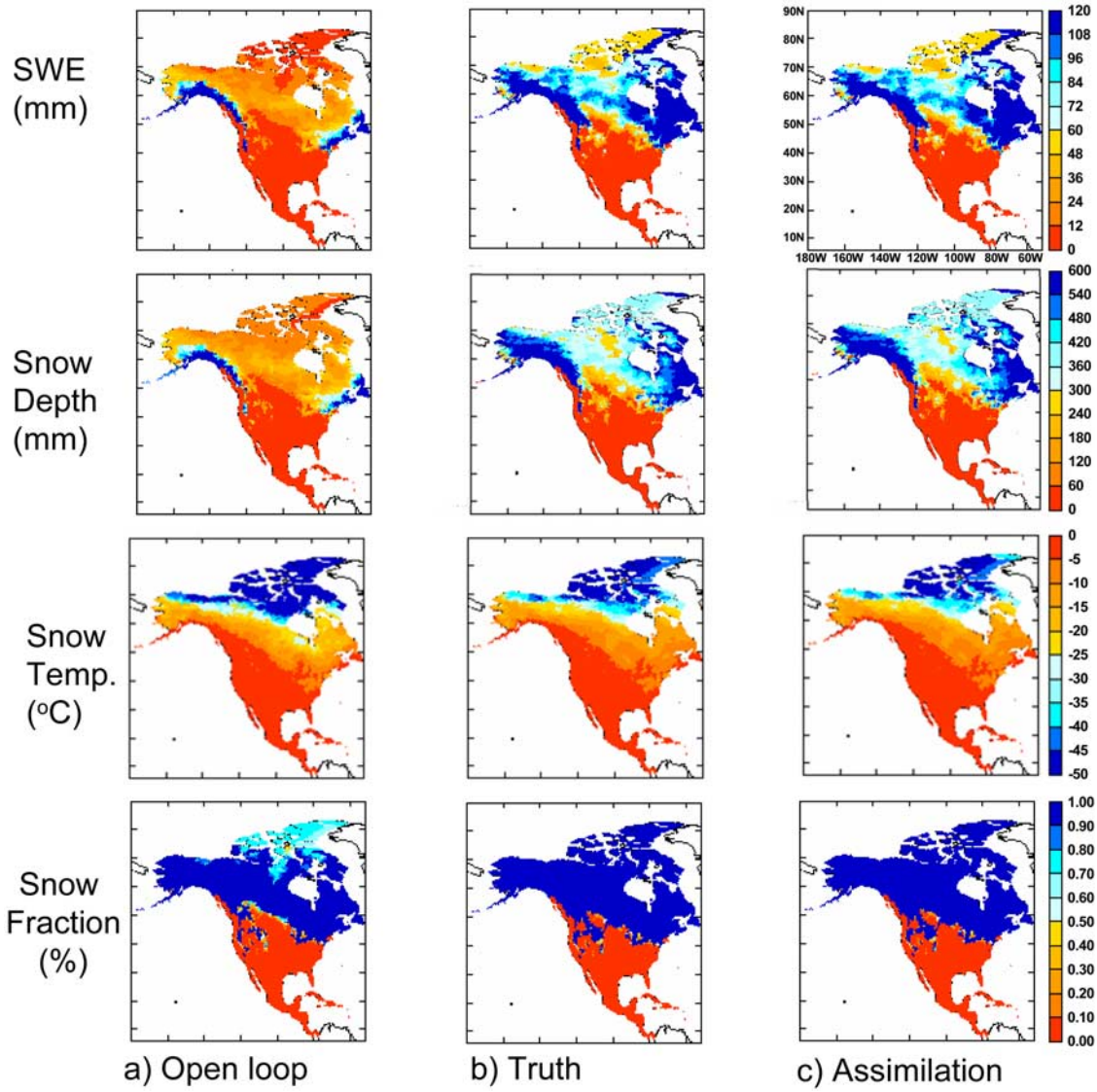

Figure 4. Same as Figure 3, except simulations are for 14 February 1987.

density and depth in the open loop run never converged to the true values.

[35] The snow temperature and snow fraction variables also maintain differences between the open loop and truth runs. While these are more subtle, they are not insignificant. It is not surprising that the assimilation is very effective in retrieving the snow water equivalent, since it is directly observed. However, the ability to also effectively retrieve the snow temperature and snow depth from this observation is significant. The snow temperature discussed here is the three-layer average, weighted by each layer's mass. It is a diagnostic variable that is a function of snow water equivalent and heat content, and while strongly coupled to the air temperature, the effect is dampened by the snowpack's thermal properties, through both the snow water equivalent and snow depth. As the snow water equivalent and/or snowpack depth increases, it provides a greater insulation to the underlying snow. In the assimilation run, the snow temperature was recovered very rapidly due to the quick recovery of snow water equivalent. In contrast, the open loop run produced a very limited snow water equivalent amount, resulting in the forecast temperature being generally colder than the true temperature, especially in northeastern Canada (Figures 3a and 4a).

[36] As an example, Figure 5 shows the snowpack evolution time series for two typical catchments. The individual snow water equivalent and snow depth time series over these two catchments clearly show how the assimilation run rapidly approached the true snow water equivalent and gradually converged to the true snow depth with time. This convergence of the snow depth with time is a direct reflection of the snow density convergence, which occurs via the model physics as the snowpack matures. In contrast, snow water equivalent, snow depth and snow density estimates in open loop runs stay below the true values throughout the three-month period.

[37] The assimilation snow forecast error location, magnitude and persistence can be seen more clearly in

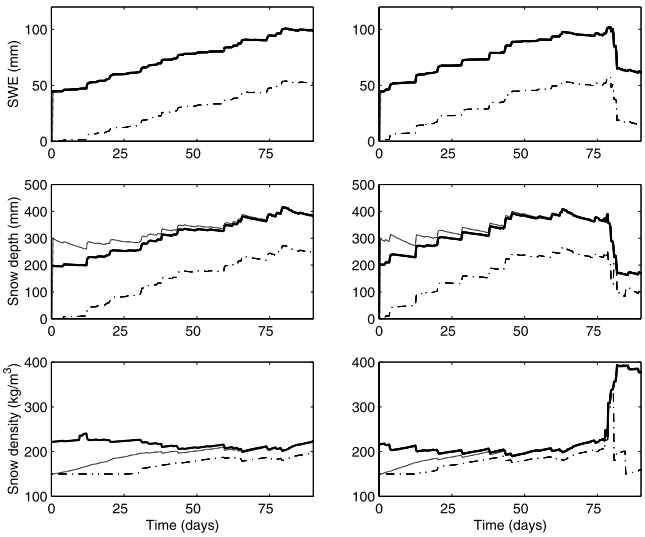

Figure 5. Snow water equivalent (top row), snow depth (middle row), and snow density (bottom row) time series for two typical catchments; the horizontal axis is time (days). The heavy line is truth, light line is assimilation, and dash-dotted line is open loop.

Figure 6, which shows assimilation error snapshots (as the difference between the assimilation and truth) on three different dates: 5 January, 14 February, and 15 March 1987. As expected, the assimilation run has very small snow water equivalent errors, since the direct observation is assimilated. The total snow water equivalent assimilation errors are likely due to numerical round off (Figure 6, top row), with the error being only a small fraction of one percent of the snow water equivalent. However, snow depth is prominently overestimated near the start of the assimilation run (5 January), due to snow density underestimation. By the middle of February, the assimilation run had recovered the snow depth in most of the areas, except for northeastern Canada. There are also some average snow temperature differences between the assimilation and truth runs near the start of the assimilation run, but these differences diminished as the assimilation run progressed. The persistent snow temperature warm bias over northeastern Canada directly reflects the increased insulating properties of the deeper snowpack forecast.

[38] Figure 7 shows the root-mean square error and mean error time series for the assimilation and open loop runs over the three-month period (January to

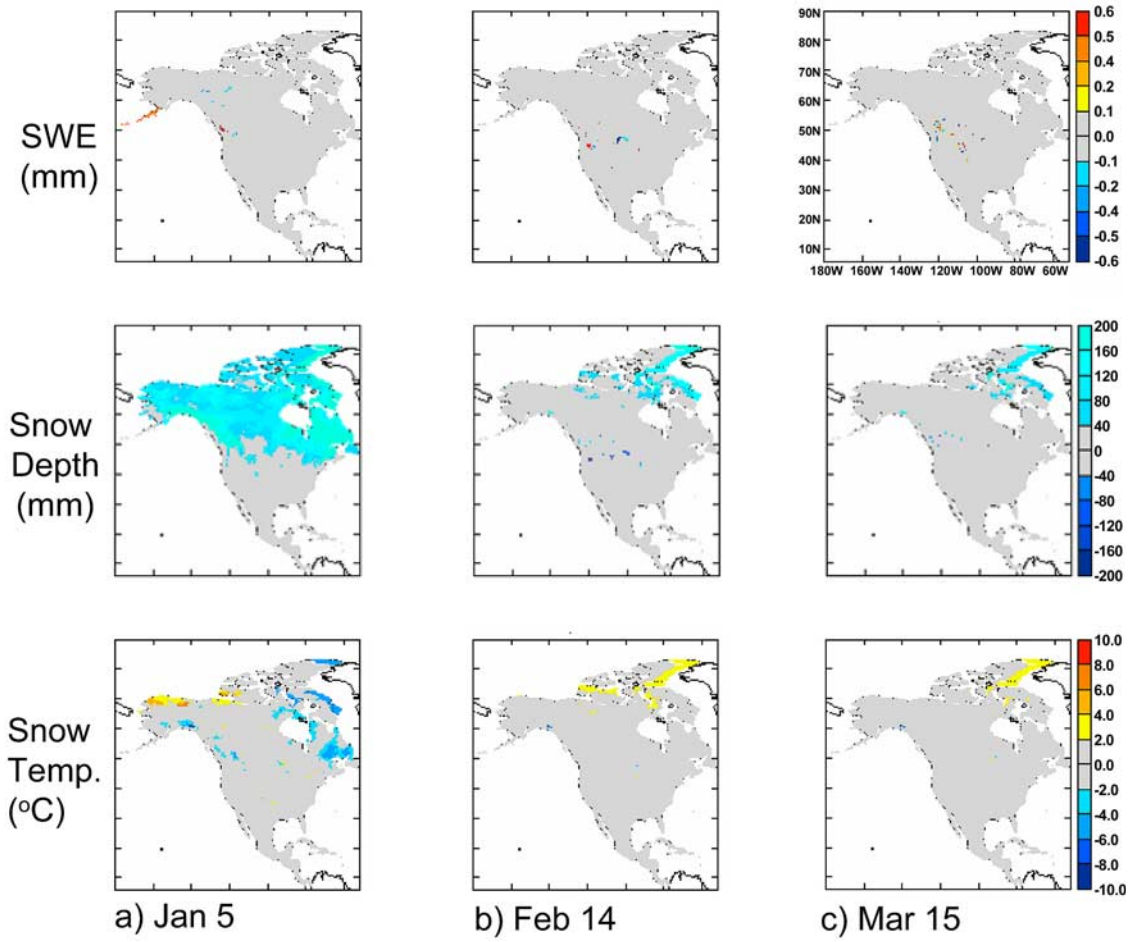

Figure 6. Snow state assimilation error (assimilation-truth) over North America: snow water equivalent (top row, in mm), snow depth (middle row, in mm), and snow temperature (bottom row, in °C) for (a) 5 January 1987, (b) 14 February 1987, and (c) 15 March 1987.

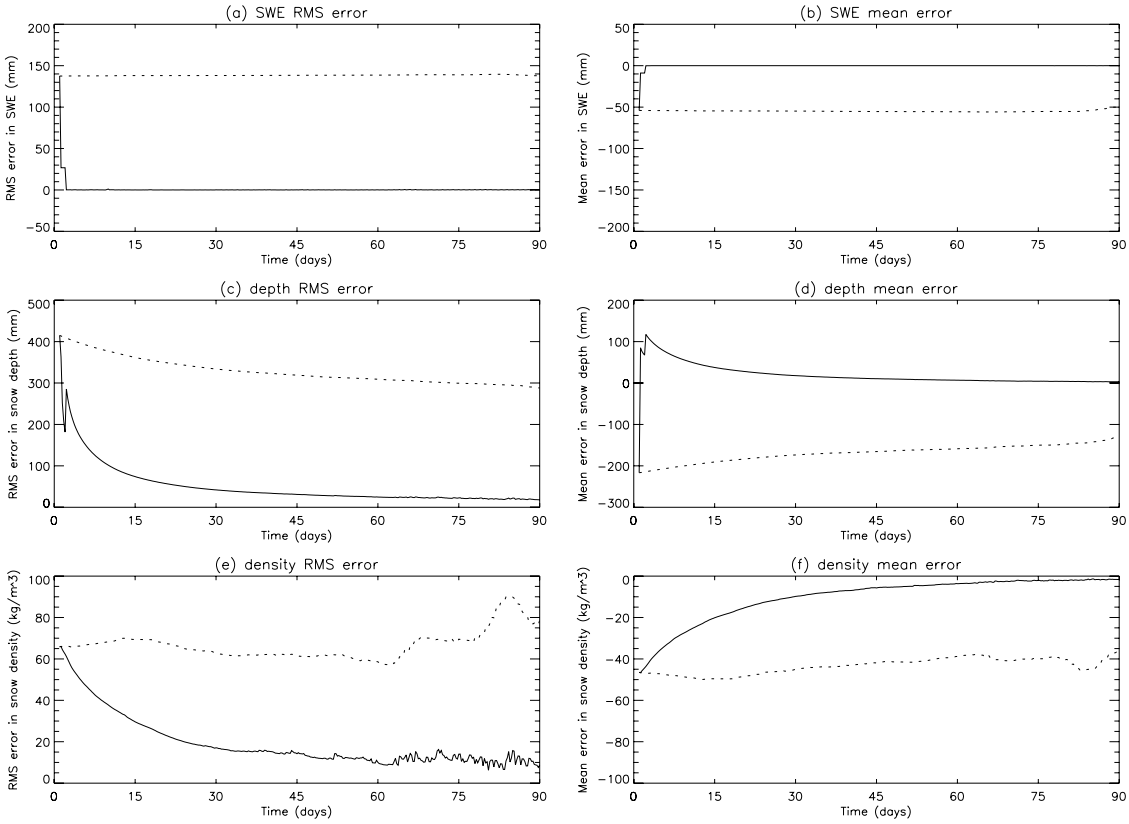

Figure 7. Root-mean square (RMS) and mean error of assimilation (solid) and open loop runs (dotted) averaged over the North American continent: (a) snow water equivalent RMS errors, (b) snow water equivalent mean errors, (c) depth RMS errors, (d) depth mean errors, (e) density RMS errors, and (f) density mean errors.

March), averaged over North America. This shows how the continental average errors in the assimilation run reduce quickly to zero, while errors in the open loop run remained unchanged for snow water equivalent, decreased slowly for snow depth, and increased for snow density. This figure again shows how there is an initial snow depth over-estimation due to a snow density under-estimation.

[39] An important motivation for snow assimilation is the potential impact on flood and climate forecasting. Hence a comparison between monthly averaged runoff and atmospheric fluxes (evapotranspiration, upward shortwave radiation and upward longwave radiation) from the open loop run and assimilation runs for February 1987 is shown in Figure 8. In general, the differences between the assimilation and truth runs are negligible (Figure 8c), while the differences between the open loop and truth runs are significant (Figure 8b), except for evapotranspiration. This is a direct result of the extremely low evapotranspiration rates at this time of the year over snow-covered northern latitudes. In comparison to the truth (Figure 8a), the assimilation impact on the snow states has significantly improved both upward shortwave and longwave radiation, which are strongly affected by snow impact on surface albedo. Because February is in the middle of the winter snow season, snowmelt-induced runoff is likely to be quite low, and hence the effects of assimilation on runoff are negligible. However, it can be seen that runoff predictions are nonetheless significantly improved by the assimilation for areas along the southern edge of the snow belt where snowmelt-induced runoff is occurring.

6. Conclusions

[40] A methodology for generating global climate model snowpack initialization that does not rely on land surface model spin-up has been described. This methodology produces the snowpack states by assimilating total snow water equivalent observations using the extended Kalman filter. A series of numerical experiments using this methodology illustrate that snowpack states (snow water equivalent, snow depth and snow temperature/heat content) may be retrieved from total snow water equivalent observations which are readily available from passive microwave remote sensing. Moreover, the effect of snowpack forecast errors on the energy and water balance (i.e., evapotranspiration, runoff and both upward longwave and shortwave radiation) has been demonstrated, with the assimilation having a significant positive impact on these flux estimates.

[41] This study has demonstrated that by assimilating total snow water equivalent observations using the extended Kalman filter, and reconstructing the other prognostic snow states (snow depth and heat content) through the use of diagnostic model variables (snow density and

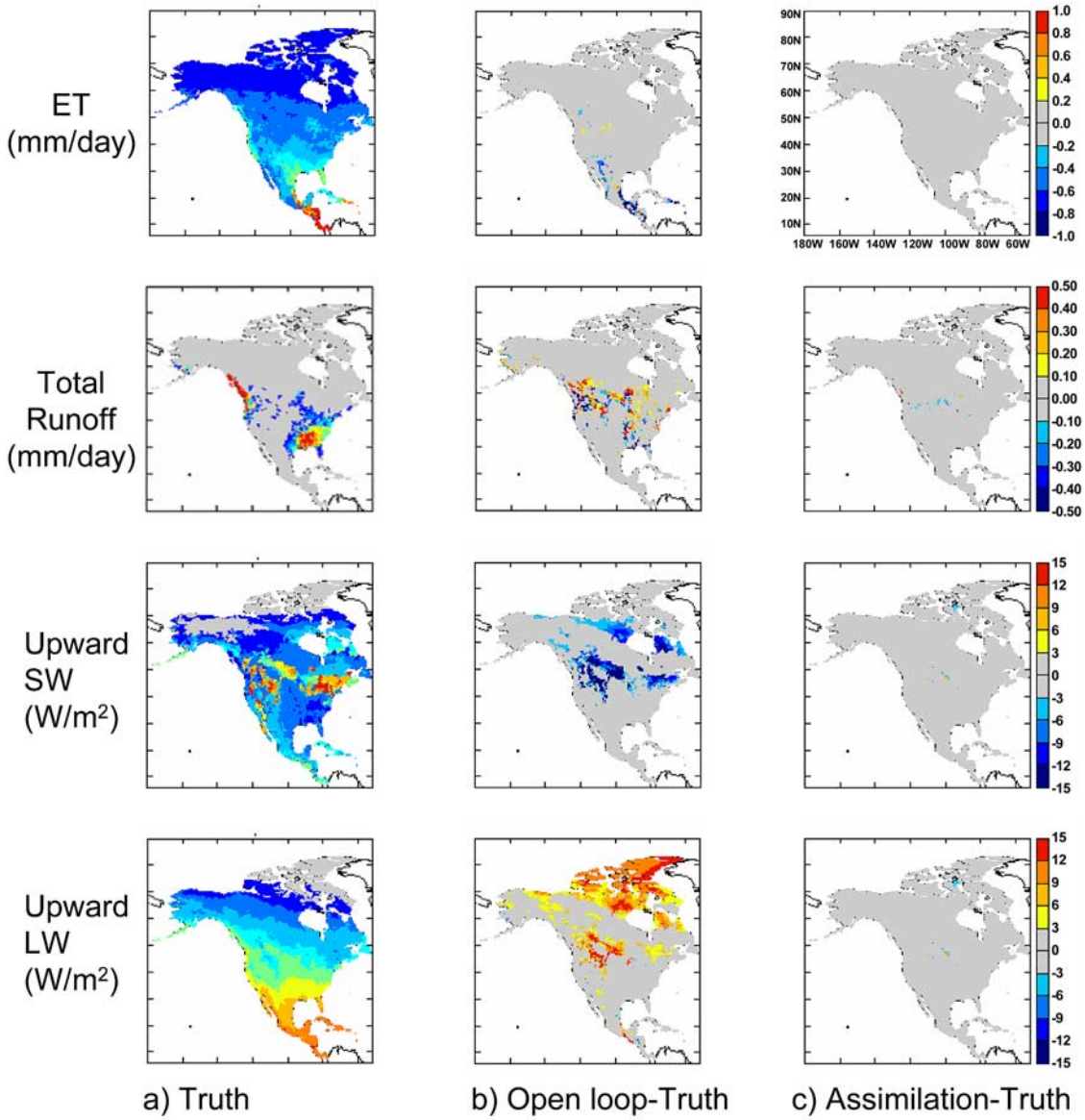

Figure 8. Monthly average evapotranspiration (in mm/day; first row), total runoff (in mm/day; second row), upward shortwave radiation (in W/m^2; third row) and upward longwave radiation (in W/m^2; fourth row), comparison for the (a) truth run, (b) open loop minus truth run, and (c) assimilation minus truth run for February 1987.

temperature), all snowpack prognostic variables can be retrieved efficiently. This is because snow water equivalent is highly correlated with snow depth and heat content, while independent of snow density and temperature. It should be noted that this twin experiment has not accounted for model simulation or observation biases, even though they are often inevitable in reality. This important issue is beyond the scope of the current paper, and is an important future research topic.

[42] **Acknowledgments.** The authors thank Randal Koster, Dick Dee, Ricardo Todling, Michael Ghil, Rolf Reichle, James Foster and Al Chang for helpful discussions during the course of this work. We also thank Marc Stieglitz and Stephen Dery for valuable discussions about the snow model and its schematic presentation in Figure 1. The comments from the three anonymous reviewers helped to improve the presentation of the paper significantly. Processing of forcing data by Aaron Berg is acknowledged. This work was supported by the National Aeronautics and Space Administration Earth Observing System Interdisciplinary Science (NASA EOS/IDS) Program NRA99-OES-04.

References

Aguado, E. (1985), Radiation balances of melting snow covers at an open site in the central Sierra Nevada, California, *Water Resour. Res.*, *21*, 1649–1654.

Baker, D. G., D. L. Ruschy, R. H. Skaggs, and D. B. Wall (1992), Air temperature and radiation depressions associated with snow cover, *J. Appl. Meteorol.*, *31*, 247–254.

Bamzai, A. S., and J. Shukla (1999), Relation between Eurasian snow cover, snow depth, and the Indian summer monsoon: An observational study, *J. Clim.*, *12*, 3117–3132.

Berg A. A., J. S. Famiglietti, J. P. Walker, and P. R. Houser (2003), Impact of bias correction to reanalysis products on simulations of North American soil moisture and hydrological fluxes, *J. Geophys. Res.*, *108*(D16), 4490, doi:10.1029/2002JD003334.

Brasnett, B. (1999), A global analysis of snow depth for numerical weather prediction, *J. Appl. Meteorol.*, *38*, 726–740.

Brown, R., B. Brasnett, and D. Robinson (2001), Development of a gridded North American monthly snow depth and snow water equivalent dataset for GCM validation, in Proceedings of the 58th Annual Meeting of Eastern Snow Conference, pp. 333–340, East. Snow Conf., Ottawa, Ont.

Brown, R., B. Brasnett, and D. Robinson (2003), Gridded North American monthly snow depth and snow water equivalent for GCM evaluation, *Atmos. Ocean*, *41*, 1–14.

Chang, A. T. C., J. L. Foster, and D. K. Hall (1987), Nimbus7 SMMR derived global snow cover parameters, *Ann. Glaciol.*, *9*, 39–44.

Cohen, J., and D. Entekhabi (1999), Eurasian snow cover variability and Northern Hemisphere climate predictability, *Geophys. Res. Lett.*, *26*, 345–348.

Dee, D. P., and A. M. da Silva (1998), Data assimilation in the presence of forecast bias, *Q. J. R. Meteorol. Soc.*, *124*, 269–295.

Dee, D. P., and R. Todling (2000), Data assimilation in the presence of forecast bias: The GEOS moisture analysis, *Mon. Weather Rev.*, *128*, 3268–3282.

Dewey, K. F. (1977), Daily maximum and minimum temperature forecasts and the influence of snow cover, *Mon. Weather Rev.*, *105*, 1594–1597.

Ducharne, A., R. D. Koster, M. J. Suarez, M. Stieglitz, and P. Kumar (2000), A catchment-based approach to modeling land surface processes in a general circulation model: 2. Parameter estimation and model demonstration, *J. Geophys. Res.*, *105*, 24,823–24,838.

Foster, J. L., A. T. C. Chang, and D. K. Hall (1997), Comparison of snow mass estimates from a prototype passive microwave snow algorithm, a revised algorithm and a snow depth climatology, *Remote Sens. Environ.*, *62*, 132–142.

Fukumori, I., R. Raghunath, L.-L. Fu, and Y. Chao (1999), Assimilation of TOPEX/Poseidon altimeter data into a global ocean circulation model: How good are the results?, *J. Geophys. Res.*, *104*, 25,647–25,665.

Gelb, A. (1974), Optimal linear filtering, in *Applied Optimal Estimation*, edited by A. Gelb, pp. 102–155, MIT Press, Cambridge, Mass.

Ghil, M., and P. Malanotte-Rizzoli (1991), Data assimilation in meteorology and oceanography, *Adv. Geophys.*, *33*, 141–266.

Groisman, P. Y., T. R. Karl, and R. W. Knight (1994), Observed impact of snow cover on the heat balance and the rise of continental spring temperatures, *Science*, *263*, 198–200.

Gutzler, P. Y., and R. D. Rosen (1995), Interannual variability of wintertime snow cover on the heat balance and the rise of continental spring temperatures, *Science*, *263*, 198–200.

Hall, D. K. (1988), Assessment of polar climate change using satellite technology, *Rev. Geophys.*, *26*, 26–39.

Hall, D. K. (1998), Remote sensing of snow and ice using imaging radar, in *Manual of Remote Sensing*, 3rd ed., pp. 677–703, Am. Soc. for Photogramm. and Remote Sens., Falls Church, Va.

Ide, K., P. Courtier, M. Ghil, and A. C. Lorenc (1997), Unified Notation for data assimilation: Operational, sequential and variational, *J. Meteorol. Soc. Jpn.*, *75*, 181–189.

Johnson, R. H., G. S. Young, and J. J. Toth (1984), Mesoscale weather effects of variable snow cover over northeast Colorado, *Mon. Weather Rev.*, *112*, 1141–1152.

Keppenne, C. L. (2000), Data assimilation into a primitive-equation model with a parallel ensemble Kalman filter, *Mon. Weather Rev.*, *128*, 1971–1981.

Koster, R. D., and M. J. Suarez (1995), Relative contributions of land and ocean processes to precipitation variability, *J. Geophys Res.*, *100*, 13,775–13,790.

Koster, R. D., M. J. Suarez, A. Ducharne, M. Stieglitz, and P. Kumar (2000), A catchment-based approach to modeling land surface processes in a general circulation model: 1. Model structure, *J. Geophys. Res.*, *105*, 24,809–24,822.

Liston, G. E., R. A. Pielke Sr., and E. M. Greene (1999), Improving first-order snow-related deficiencies in a regional climate model, *J. Geophys. Res.*, *104*, 19,559–19,567.

Lo, F., and M. P. Clark (2002), Relationships between spring snow mass and summer precipitation in the southwestern United States associated with the North American monsoon system, *J. Clim.*, *15*, 1378–1385.

Lynch-Stieglitz, M. (1994), The development and validation of a simple snow model for the GISS GCM, *J. Clim.*, *7*, 1842–1855.

Miller, R. N., M. Ghil, and F. Gauthiez (1994), Advanced data assimilation in strongly nonlinear dynamical systems, *J. Atmos. Sci.*, *51*, 1037–1056.

Mitchell, K., et al. (2002), Reducing near-surface cool/moist biases over snowpack and early spring wet soils in NCEP ETA model forecasts via land surface model upgrades, in *Proceedings of the 16th Conference on Hydrology and 13th Symposium on Global Change and Climate Variations*, pp. J1–J6, Am. Meteorol. Soc., Boston, Mass.

Namias, J. (1985), Some empirical evidence for the influence of snow cover on temperature and precipitation, *Mon. Weather Rev.*, *113*, 1542–1553.

Robinson, D. A. (2002), Developing a blended continental snow cover dataset, in *Proceedings of the 16th Conference on Probability and Statistics in the Atmospheric Sciences and the Symposium on Observations, Data Assimilation, and Probabilistic Prediction*, pp. 87–88, Am. Meteorol. Soc., Boston, Mass.

Robinson, D. A., and G. Kukla (1985), Maximum surface albedo of seasonally snow-covered lands in the Northern Hemisphere, *J. Clim. Appl. Meteorol.*, *24*, 402–411.

Robinson, D. A., K. F. Dewey, and R. R. Heim (1993), Global snow cover monitoring: An update, *Bull. Am. Meteorol. Soc.*, *74*, 1689–1696.

Rodell, M., et al. (2004), The Global Land Data Assimilation System, *Bull. Am. Meteorol. Soc.*, *85*(3), 381–394.

Sellers, P. J., J. Collatz, and F. G. Hall (1996), The ISLSCP Initiative I global data sets: Surface boundary conditions and atmospheric forcings for land-atmosphere studies, *Bull. Am. Meteorol. Soc.*, *77*, 1987–2005.

Stieglitz, M., A. Ducharne, R. Koster, and M. Suarez (2001), The impact of detailed snow physics on the simulation of snow cover and subsurface thermodynamics at continental scales, *J. Hydrometeorol.*, *2*, 228–242.

Sud, Y. C., and D. M. Mocko (1999), New Snow-physics to complement SSiB. Part I: Design and evaluation with ISLSCP Initiative I datasets, *J. Meteorol. Soc. Jpn.*, *77*(1B), 335–348.

Sun, C., Z. Hao, M. Ghil, and J. D. Neelin (2002), Data assimilation for a coupled ocean-atmosphere model. Part I: Sequential state estimation, *Mon. Weather Rev.*, *130*, 1073–1099.

Verron, J., L. Gourdeau, D. T. Pham, R. Murtugudde, and A. J. Busalacchi (1999), An extended Kalman filter to assimilate satellite altimeter data into a nonlinear numerical model of the tropical Pacific Ocean: Method and validation, *J. Geophys. Res.*, *104*, 5441–5458.

Verseghy, D. L. (1991), CLASS—A Canadian land surface scheme for GCMS. I: Soil model, *Int. J. Climatol.*, *11*, 111–133.

Walker, J. P., and P. R. Houser (2001), A methodology for initializing soil moisture in a global climate model: Assimilation of near-surface soil moisture observations, *J. Geophys. Res.*, *106*, 11,761–11,774.

P. R. Houser, Hydrological Sciences Branch, Laboratory for Hydrospheric Processes, NASA Goddard Space Flight Center, Greenbelt, MD 20771, USA.

C. Sun, Code 900.3, Global Modeling and Assimilation Office, NASA Goddard Space Flight Center, Greenbelt, MD 20771, USA. (csun@janus.gsfc.nasa.gov)

J. P. Walker, Department of Civil and Environmental Engineering, University of Melbourne, Parkville, Victoria 3010, Australia.